Relation between Heat of Vaporization, Ion Transport, Molar Volume, and Cation−Anion Binding Energy for Ionic Liquids

Oleg Borodin*

Wasatch Molecular Inc., 2141 St. Marys Drive, Suite 102, Salt Lake City, Utah 84108, and Department of Materials Science & Engineering, 122 South Central Campus Drive, Room 304, University of Utah, Salt Lake City, Utah 84112-0560

Received: June 26, 2009

A number of correlations between heat of vaporization (H_{vap}), cation−anion binding energy ($E_{\pm}$), molar volume (V_m), self-diffusion coefficient (D), and ionic conductivity for 29 ionic liquids have been investigated using molecular dynamics (MD) simulations that employed accurate and validated many-body polarizable force fields. A significant correlation between D and H_{vap} has been found, while the best correlation was found for $-\log(DV_m)$ vs $H_{vap} + 0.28E_{\pm}$. A combination of enthalpy of vaporization and a fraction of the cation−anion binding energy was suggested as a measure of the effective cohesive energy for ionic liquids. A deviation of some ILs from the reported master curve is explained based upon ion packing and proposed diffusion pathways. No general correlations were found between the ion diffusion coefficient and molecular volume or the diffusion coefficient and cation/anion binding energy.

Introduction

Ionic liquids (ILs) are salts typically comprised from the combination of large organic cations with various substituents (alkyls, oligoethers, etc.) and inorganic or organic anions.[1−3] ILs have attracted significant attention because of their negligible vapor pressure, high solvating capacity for organic, organometallic, and inorganic compounds, wide electrochemical stability, and thermal windows.[1] Importantly, IL properties can be tailored for specific chemical (separation, catalysis, reactions, propellants, explosives) or electrochemical (battery, actuators, supercapacitors) applications by tuning the combination of cations and anions to achieve the desired thermodynamic, solvating, and transport properties. The negligible vapor pressure of ILs is often cited as the most desirable IL attribute that leads to reduction or prevention of the solvent emissions making processing "green". The other highly desirable property of ILs is their acceptably low viscosity and high ion conductivity at or near room temperature. While viscosity and conductivity of ILs have been extensively investigated and are widely available, the experimental studies of IL heat of vaporization (H_{vap}) have proved to be challenging and have been performed only for a relatively small number of ILs.[4−10] Verevkin[8] has successfully correlated H_{vap} with a term containing IL surface tension and molar volume for 15 ILs, but little is known about the relationship between IL transport properties and H_{vap} from experiments because of lack of extensive and reliable experimental data. MD simulations are a complementary methodology that allows IL property prediction provided an accurate force field is imployed. While many heats of vaporization were reported in a number of MD simulation studies,[11−21] most of them dealt only with a few ILs and did not generate enough data to meaningfully consider relations between heat of vaporization and transport properties.

This situation is in a stark contrast to extensive correlations between temperature dependence of viscosity and H_{vap} performed for a wide range of polar, nonpolar, organic, and inorganic liquids,[22,23] utilizing various modifications of Eyring's absolute rate theory. The temperature dependence of viscosity is usually expressed using eq 1.

$$\eta V_m \sim RT \exp(\alpha H_{vap}/RT) \quad (1)$$

where η is the liquid viscosity; T is temperature; R is the gas constant; V_m is the molar volume; and α is the proportionality factor. Interestingly, the α proportionality factor shows little variation within the same class of liquids. For example, for 35 saturated, unsaturated, and cyclic hydrocarbon liquids, α ranged from 0.162 to 0.244.[22] These observations suggest that for the same class of liquids H_{vap} is strongly correlated with the activation energy for viscosity and the barrier height that molecules should overcome to diffuse/rotate. In light of this work, a number of questions as to the relationship between ion transport in IL and thermodynamic properties arise such as how much the α parameter in eq 1 varies for ILs and whether H_{vap} is at all a relevant property to correlate with the IL transport properties or whether the energy (or enthalpy) of vaporization plus a fraction of the energy of breaking the cation−anion ion pairs should be used instead of H_{vap}.

The aim of this report is to obtain insight into the relation between ion transport and IL thermodynamic properties in general and H_{vap}, in particular. In addition, we also investigate a relation between the magnitude of the cation−anion interactions and IL molar volume and IL transport following previous work by Tsuzuki et al.[24] and Slattery et al.[25]

Results and Discussion

Extensive molecular dynamics (MD) simulations of 29 ILs (see Table 1) were performed at 393 K, 333 K, and 298 K. Details of the many-body polarizable force field parametrization and MD simulations are given in our previous publication[26] and are summarized in the Supporting Information. Here we note

* Corresponding author. E-mail: oleg.borodin@utah.edu.

10.1021/jp9070357 CCC: $40.75
Published on Web 08/19/2009

TABLE 1: List of Simulated Ionic Liquids[a]

#	cation	anion	#	cation	anion
1	emim	CF_3BF_3	16	bmim	CF_3SO_3
2	emim	BF_4	17	N_{1114}	Ntf_2
3	bmim	BF_4	18	$piperid_{14}$	Ntf_2
4	bmim	PF_6	19	$morph_{14}$	Ntf_2
5	$pyrid_4$	BF_4	20	emim	$C_4H_9SO_3$
6	emim	CH_3BF_3	21	emim	FSI
7	emim	Ntf_2	22	pyr_{13}	FSI
8	bmim	Ntf_2	23	emim	$N(CN)_2$
9	EO_2mim	Ntf_2	24	bmim	$N(CN)_2$
10	bmmim	Ntf_2	25	pyr_{12}	$N(CN)_2$
11	$pyr_{1,1o2}$	Ntf_2	26	emim	$C(CN)_3$
12	$pyrid_4$	Ntf_2	27	$phosph_{12}$	$C(CN)_3$
13	c_6mim	Ntf_2	28	emim	$B(CN)_4$
14	pyr_{13}	Ntf_2	29	bmim	NO_3
15	pyr_{14}	Ntf_2			

[a] pyr_{nm} = *N*-C_n-*N*-$C_m$pyrrolidinium; for example, pyr_{13} = *N*-methyl-*N*-propylpyrrolidinium, $morph_{14}$ = *N*-methyl-*N*-propylmorpholinium, $piperid_{14}$ = *N*-methyl-*N*-butylpiperidinium, $pyr_{1,1o2}$ = *N*-methyl-*N*-(CH_3-OC_2H_4-)-pyrrolidinium, $pyrid_4$ = *N*-butylpyridinium, $phosph_{12}$ = *P*-methyl-*P*-ethylphospholanium, EO_2mim = 1-$CH_3(OCH_2CH_2)_2$-3-methylimidazolium, where EO_2 indicates two ether oxygen repeat units methyl terminated, bmmim = 1-butyl-2-methyl-3-methylimidazolium, Ntf_2 = TFSI = $N(SO_2CF_3)_2$, FSI = $N(SO_2F)_2$.

that the length of production runs was always long enough to achieve the diffusive regime in ILs and ranged from 4 to 64 ns. An excellent prediction of ion self-diffusion coefficient, conductivity, and H_{vap} was achieved.[26] The largest deviation of ion self-diffusion coefficient was about 35% from experiments.

The ion self-diffusion coefficients, conductivity, heat of vaporization, and the cation−anion binding energies were extracted from MD simulations. Enthalpy of vaporization H_{vap} was calculated using eq 2

$$H_{vap}=E_{gas} - E_{liq.} + RT \quad (2)$$

where E_{gas} is the average molar energy of the cation−anion ion pair; E_{liq} is the average molar energy of ionic liquid in the liquid state at temperature T; and R is the universal gas constant. The approximation of the gas-phase energy with the cation−anion binding energy is consistent with experimental[10] and simulation[15] evidence for simulated ILs. We do not expect an imidazolium proton to transfer and form neutral species in the gas phase as was predicted from quantum chemistry calculations for triazolium-based ILs.[27] Viscosity was also extracted from MD simulations for a few simulated ILs and compared with experiments;[26] however, many of the simulation runs at low temperature were not sufficiently long to obtain a converged viscosity value, therefore in this contribution we use the self-diffusion coefficients and conductivity as indicators of IL transport because they could be reliably extracted from MD simulations at all simulated temperatures.

Using the Stokes−Einstein relation $D \sim RT(\eta r_s)^{-1}$, where r_s is the Stokes radius of the ion,[28] and assuming $r_s \sim V_m^{1/3}$ on average, where V_m is the volume of ionic liquid per ion pair, we obtain from eq 1 the following relation

$$(V_m^{-2/3}D)^{-1} \sim \exp(\alpha H_{vap}/RT) \quad (3)$$

Thus, $(V_m^{-2/3}D)^{-1}$ activation energy is expected to be related to αH_{vap} if an analogy with simple liquids holds. Moreover, because temperature dependence of diffusion is much stronger, the activation energy for $(V_m^{-2/3}D)^{-1}$ could be approximated with the diffusion coefficient activation energy. We begin, however, by examining a relation between the logarithm of average ion self-diffusion coefficient (D) at 298 K and its activation energy (E_D) calculated for the region 298−393 K assuming an Arrhenius behavior. An activation energy E_D was obtained by fitting three data points at 393, 333, and 298 K using Arrhenius behavior without any weights. Figure 1 shows an intriguing linear relationship between $\log(1/D)$ vs E_D. This behavior is consistent with the supposition that at very high temperature these ILs will have similar self-diffusion coefficients, and the value of the self-diffusion coefficient at room temperature is largely determined by the activation energy.

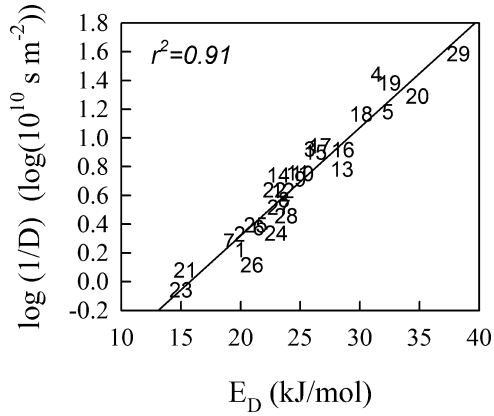

Figure 1. Dependence of the ion average self-diffusion coefficient (D) at 298 K on the activation energy for the self-diffusion coefficient (E_D) for 29 ILs listed in Table 1. r^2 is the coefficient of determination.

We proceed with an investigation of the relation between D vs H_{vap} as shown in Figure 2a. A correlation between D and H_{vap} is observed. The quality of the correlation becomes especially good if only Ntf_2-based ionic liquids are considered as shown in the inset for Figure 2a. A similar correlation has been found between ionic conductivity and H_{vap} as shown in Figure 3 and for E_D vs H_{vap} as shown in the Supporting Information. If ions were to diffuse as ion pairs in ILs, their vaporization into the gas phase would be analogous to liquids. However, the dynamic degree of ion correlation is typically low in the range of 0.3−0.5,[29] and ionic pairs do not exist over long times in ILs, thus one can argue that the strength of the cation−anion binding energy should also be related to ion transport as discussed by Tsuzuki et al.[24] Attempts to improve a correlation between $-\log(D)$ and H_{vap} by adding a fraction of the cation−anion binding energy revealed that the overall correlation could be improved if 0.18 of the gas-phase cation−anion binding energy ($E_\pm$) is added to H_{vap} as shown in Figure 2b. A qualitatively similar behavior was obtained for E_D (see Supporting Information). The sum $H_{vap} + 0.18E_\pm$ could be thought of as an effective cohesive energy that reflects contributions due to removing an ion pair from IL and breaking it apart.

A more detailed investigation of Figure 2b reveals that five ILs based upon $N(CN)_2^-$ and $C(CN)_3^-$ fall on the same curve, while this was not the case for the $\log(D)$ vs H_{vap} correlation shown in Figure 2a. To clearly show the correlations for various classes of ILs, we grouped them together as shown in Figure 4 following suggestions from Slattery et al.[25] The Ntf_2^- anion-based ILs lie on a line with an exception of two ILs containing $bmmim^+$ and EO_2mim^+ cations (ILs #9 and #10) that show some deviations. The FSI-based ILs and ILs containing $N(CN)_2^-$ and

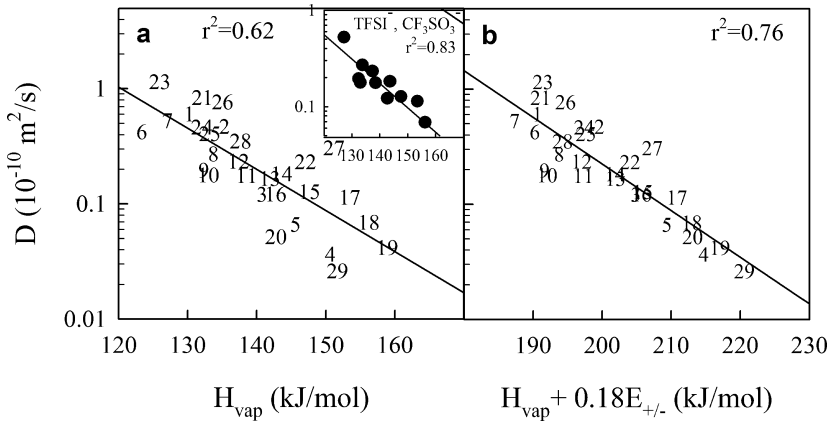

Figure 2. Correlation between the ion average self-diffusion coefficient (D) and enthalpy of vaporization (H_{vap}) and cation−anion binding energy ($E_\pm$) at 298 K. r^2 is the coefficient of determination.

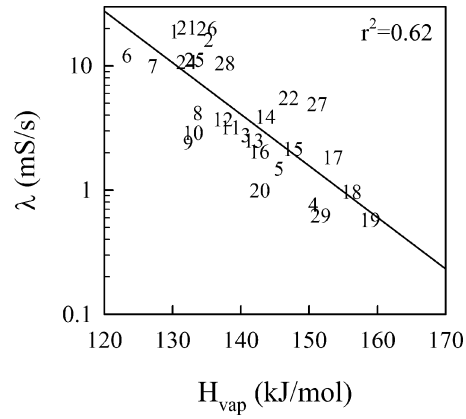

Figure 3. Correlation between ionic conductivity and enthalpy of vaporization (H_{vap}).

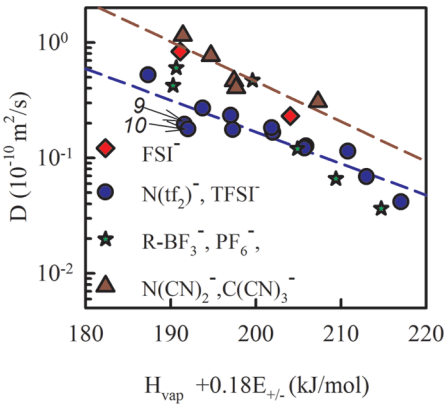

Figure 4. Correlation between ion average self-diffusion coefficient (D) and enthalpy of vaporization (H_{vap}) and cation−anion binding energy $E_\pm$ at 298 K.

$C(CN)_3^-$ are shifted to higher ion self-diffusion coefficients compared to the Ntf_2-anion-based ILs, thus indicating a faster transport for $N(CN)_2^-$, $C(CN)_3^-$, and FSI-based ILs for the same effective cohesive energy compared to the Ntf_2-anion-based ILs. The $N(CN)_2^-$, $C(CN)_3^-$, and FSI^- anions are smaller than the Ntf_2^- anion suggesting that smaller ions yield faster ion transport at the same effective cohesive energy. Our attempts to correlate a product of the ion average self-diffusion coefficient D and a volume of the ion pair in power n (V_m^n) revealed that the best correlation is obtained for $(V_mD)^{-1}$ vs $H_{vap} + 0.28E_\pm$ as shown in Figure 5. This correlation is noticeably better than correlations

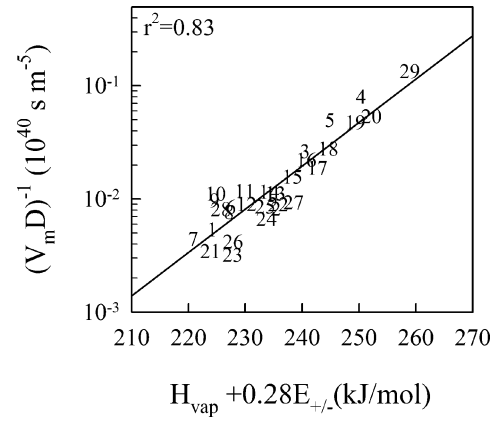

Figure 5. Correlation between the ion average self-diffusion coefficient (D) multiplied by volume of the ion pair vs enthalpy of vaporization (H_{vap}) + 28% of cation−anion binding energy $E_\pm$ at 298 K.

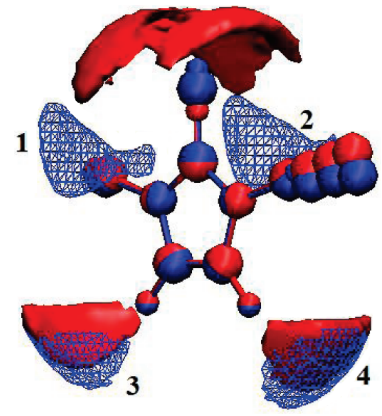

Figure 6. Isosurface of O atom of Ntf_2^- anions around $bmim^+$ for $\rho/\rho^{random} = 9$ (volume distribution function yielding nine times the bulk average oxygen atom density) for [bmim][Ntf_2] (red) and [mmbim][Ntf_2] (blue) at 298 K. Average atom positions of the $bmim^+$ cation are shown.

shown in Figures 2 and 4 and allows, to a large extent, to bring data for all ILs on the universal same curve with two exceptions.

The largest deviations in Figure 5 are observed for two ILs containing $bmmim^+$ and EO_2mim^+ cations (ILs #9 and #10) as was seen in Figure 4. What makes ion diffusion different for these two cations as opposed to C_nmim^+, pyr_{1n}^+, $pirid_4^+$, $piperid_{14}$, or $morph_{14}^+$ that lie on the same curve? To answer this question, a distribution of the oxygen atom

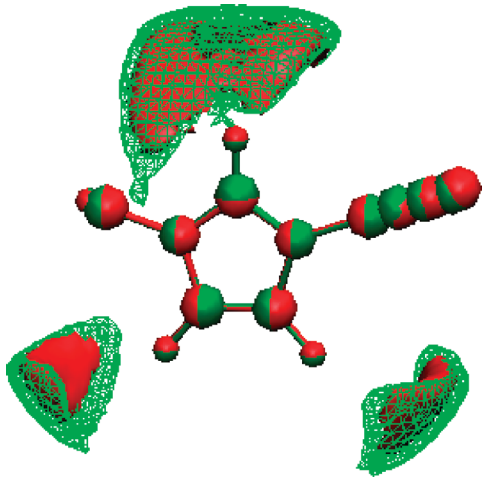

Figure 7. Isosurface of O atom of Ntf_2^- anions around $bmim^+$ for $\rho/\rho^{random} = 9$ (volume distribution function yielding nine times the bulk average oxygen atom density) for [bmim][Ntf_2] (red solid surface) and [bmim][$N(CN)_2$] (green wireframe) at 298 K. Average atom positions of the $bmim^+$ cation are shown.

of the Ntf_2^- anion around $bmim^+$ and $bmmim^+$ cations has been calculated and is shown in Figure 6 and in the Supporting Information, Figure S3, for three additional projections. Methylation of $C_{(2)}$ hydrogen ($bmim^+ \rightarrow bmmim^+$) significantly changes the location of the Ntf_2^- anion near the $C_{(2)}$ carbon of the $bmim^+$ cation denoted with numbers 1 and 2 in Figure 6. In [bmmim][Ntf_2], oxygen atoms of Ntf_2^- are located in two clearly separated regions 1 and 2 instead of occupying a broad region located directly above the $C_{(2)}$ carbon as is the case for [bmim][Ntf_2]. Thus, a pathway for relaxation associated with the anion moving over the $C_{(2)}$–H group (from region 1 to 2 and back) is disrupted in $bmmim^+$ resulting in a change of the diffusion mechanism and slower diffusion in [bmmim][Ntf_2] compared to [bmim][Ntf_2] despite slightly (by 0.7 kcal/mol) lower H_{vap} for [bmmim][Ntf_2] compared to [bmim][Ntf_2].

The other outlier in Figures 2–5 is the [EO_2mim][Ntf_2] IL. In this IL, an oligoether group strongly interacts with the C–H groups from the imidazolium ring, thus decreasing an effective cation size and lowering H_{vap} due to self-interaction.[30] These observations for [bmmim][Ntf_2] and [EO_2mim][Ntf_2] ILs suggest that significant changes in the ionic liquid relaxation pathways are likely to lead to deviations from the observed correlations between ion transport properties and H_{vap} (Figure 5). Naturally, a question about the similarity of diffusion pathways for ILs with various anions arises. Investigation of the anion distribution around the cation provides insight into ion packing and possible diffusion pathways. Figure 7 compares anion distribution around the $bmim^+$ cation for two quite different anions Ntf_2^- and $N(CN)_2^-$. Despite the difference in size and shape of these two anions, the coordination of O from Ntf_2 and terminal nitrogen atoms from $N(CN)_2^-$ around $bmim^+$ is quite similar suggesting that the diffusion pathways would be similar. A slightly more diffuse distribution for $N(CN)_2^-$ compared to Ntf_2^- around the $bmim^+$ cation is likely attributed to a faster dynamics for [bmim][$N(CN)_2$] IL compared to Ntf_2-based ILs as seen in Figure 5.

In the previous quantum chemistry study, Tsuzuki et al.[24] attempted to correlate the cation–anion binding energy with the IL conductivity with limited success. The presence of such correlations would allow fast screening of ILs based upon gas phase quantum chemistry calculations. Unfortunately, no correlation between the ion diffusion and the cation–anion binding energy was found as shown in Figure 8a indicating that quantum chemistry studies of the cation–anion ion pairs are unlikely to yield useful trends for predicting ionic conductivity. In a separate work, Slattery et al.[25] investigated a correlation between ion transport and molar volume. A plot of ion diffusion vs ion pair volume is shown in Figure 8b. Only correlations for a small subset of ILs such as [emim][Ntf_2], [bmim][Ntf_2], [C_6mim][Ntf_2], and [EO_2mim][Ntf_2] were found as shown with dashed lines.

Conclusions

A relation between ion transport properties, heat of vaporization, molar volume, and cation–anion binding energies has been studied. A significant correlation between ion transport and heat of vaporization has been found indicating that attempts to synthesize novel ILs with an enhanced transport are likely to result in more volatile ILs with lower H_{vap}. The correlation between ion self-diffusion coefficient and thermodynamic and energetic parameters was shown to further improve when the molar volume and cation–anion binding energy are incorporated in the correlation as shown in Figure 5. This correlation gives another alternative to predicting heat of vaporization for ionic liquids that is difficult to predict experimentally.

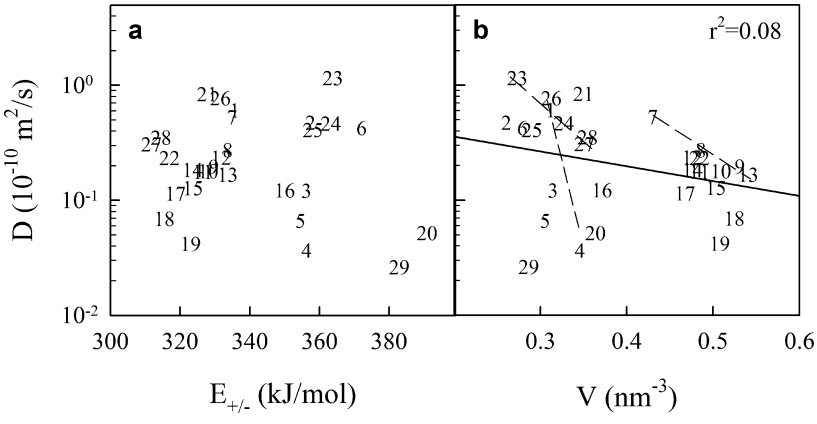

Figure 8. Correlation between the ion average self-diffusion coefficient (D), cation–anion binding energy $E_{\pm}$, and ionic liquid volume per ion pair at 298 K.

Acknowledgment. Financial support of this work by Air Force Office of Scientific Research (FA9550-09-C-0110) and DOE Contract No. DE-AC02-05CH11231 on PO No. 6838611 is acknowledged.

Supporting Information Available: Length of production runs, a table with self-diffusion coefficients, conductivities, and heats of vaporization. This material is available free of charge via the Internet at http://pubs.acs.org.

References and Notes

(1) Plechkova, N. V.; Seddon, K. R. *Chem. Soc. Rev.* **2008**, *37*, 123–150.
(2) Gardas, R. L.; Coutinho, J. A. P. *AIChE J.* **2009**, *55*, 1274–1290.
(3) Xue, H.; Verma, R.; Shreeve, J. M. *J. Fluorine Chem.* **2006**, *127*, 159–176.
(4) Zaitsau, D. H.; Kabo, G. J.; Strechan, A. A.; Paulechka, Y. U.; Tschersich, A.; Verevkin, S. P.; Heintz, A. *J. Phys. Chem. A* **2006**, *110*, 7303–7306.
(5) Emel'yanenko, V. N.; Verevkin, S. P.; Heintz, A. *J. Am. Chem. Soc.* **2007**, *129*, 3930–3937.
(6) Emel'yanenko, V. N.; Verevkin, S. P.; Heintz, A.; Corfield, J. A.; Deyko, A.; Lovelock, K. R. J.; Licence, P.; Jones, R. G. *J. Phys. Chem. B* **2008**, *112*, 11734–11742.
(7) Emel'yanenko, V. N.; Verevkin, S. P.; Heintz, A.; Schick, C. *J. Phys. Chem. B* **2008**, *112*, 8095–8098.
(8) Verevkin, S. P. *Angew. Chem., Int. Ed.* **2008**, *47*, 5071–5074.
(9) Santos, L. M. N. B. F.; Lopes, J. N. C.; Coutinho, J. A. P.; Esperanca, J. M. S. S.; Gomes, L. R.; Marrucho, I. M.; Rebelo, L. P. N. *J. Am. Chem. Soc.* **2007**, *129*, 284–285.
(10) Armstrong, J. P.; Hurst, C.; Jones, R. G.; Licence, P.; Lovelock, K. R. J.; Satterley, C. J.; Villar-Garcia, I. J. *Phys. Chem. Chem. Phys.* **2007**, *9*, 982–990.
(11) Wu, X. P.; Liu, Z. P.; Huang, S. P.; Wang, W. C. *Phys. Chem. Chem. Phys.* **2005**, *7*, 2771–2779.
(12) Cadena, C. *Molecular Modeling of the Thermophysical and Transport Properties of Ionic Liquids*; University of Notre Dame, 2006.
(13) Liu, Z. P.; Wu, X. P.; Wang, W. C. *Phys. Chem. Chem. Phys.* **2006**, *8*, 1096–1104.
(14) Micaelo, N. M.; Baptista, A. M.; Soares, C. M. *J. Phys. Chem. B* **2006**, *110*, 14444–14451.
(15) Kelkar, M. S.; Maginn, E. J. *J. Phys. Chem. B* **2007**, *111*, 9424–9427.
(16) Koddermann, T.; Paschek, D.; Ludwig, R. *ChemPhysChem* **2007**, *8*, 2464–2470.
(17) Rebelo, L. P. N.; Lopes, J. N. C.; Esperan, J. M. S. S.; Guedes, H. J. R.; £achwa, J.; Visak, V. N.; Visak, Z. P. *Acc. Chem. Res.* **2007**, *40*, 1114–1121.
(18) Kelkar, M. S.; Shi, W.; Maginn, E. J. *Ind. Eng. Chem. Res.* **2008**, *47*, 9115–9126.
(19) Ludwig, R. *Phys. Chem. Chem. Phys.* **2008**, *10*, 4333–4339.
(20) Raabe, G.; Koehler, J. *J. Chem. Phys.* **2008**, *128*, 154509.
(21) Sambasivarao, S. V.; Acevedo, O. *J. Chem. Theory Comput.* **2009**, *5*, 1038–1050.
(22) Qun-Fang, L.; Yu-Chun, H.; Rui-Sen, L. *Fluid Phase Equilib.* **1997**, *140*, 221–231.
(23) Macias-Salinas, R.; Garcia-Sanchez, F.; Hernandez-Garduza, O. *AIChE J.* **2003**, *49*, 799–804.
(24) Tsuzuki, S.; Tokuda, H.; Hayamizu, K.; Watanabe, M. *J. Phys. Chem. B* **2005**, *109*, 16474–16481.
(25) Slattery, J. M.; Daguenet, C.; Dyson, P. J.; Schubert, T. J. S.; Krossing, I. *Angew. Chem., Int. Ed.* **2007**, *46*, 5384–5388.
(26) Borodin, O. *J. Phys. Chem. B* **2009**, *113*, 11463−11478.
(27) Schmidt, M. W.; Gordon, M. S.; Boatz, J. A. *J. Chem. Phys. A* **2005**, *109*, 7285–7295.
(28) Tokuda, H.; Hayamizu, K.; Ishii, K.; Abu Bin Hasan Susan, M.; Watanabe, M. *J. Phys. Chem. B* **2004**, *108*, 16593–16600.
(29) Tokuda, H.; Tsuzuki, S.; Susan, M. A. B. H.; Hayamizu, K.; Watanabe, M. *J. Phys. Chem. B* **2006**, *110*, 19593–19600.
(30) Smith, G. D.; Borodin, O.; Li, L.; Kim, H.; Liu, Q.; Bara, J. E.; Gin, D. L.; Nobel, R. *Phys. Chem. Chem. Phys.* **2008**, *10*, 6301–6312.

JP9070357